MAGNETIC RESONANCE IN MEDICINE

Toward a Quantitative Assessment of Diffusion Anisotropy

Carlo Pierpaoli, Peter J. Basser

Indices of diffusion anisotropy calculated from diffusion coefficients acquired in two or three perpendicular directions are rotationally variant. In living monkey brain, these indices severely underestimate the degree of diffusion anisotropy. New indices calculated from the entire diffusion tensor are rotationally invariant (RI). They show that anisotropy is highly variable in different white matter regions depending on the degree of coherence of fiber tract directions. In structures with a regular, parallel fiber arrangement, water diffusivity in the direction parallel to the fibers ($D_{\parallel} \approx 1400$–$1800 \times 10^{-6}$ mm^2/s) is almost 10 times higher than the average diffusivity in directions perpendicular to them ($(D + D\perp')/2 \approx 150$–$300 \times 10^{-6}$ mm^2/s), and is almost three times higher than previously reported. In structures where the fiber pattern is less coherent (e.g., where fiber bundles merge), diffusion anisotropy is significantly reduced. However, RI anisotropy indices are still susceptible to noise contamination. Monte Carlo simulations show that these indices are statistically biased, particularly those requiring sorting of the eigenvalues of the diffusion tensor based on their magnitude. A new intervoxel anisotropy index is proposed that locally averages inner products between diffusion tensors in neighboring voxels. This "lattice" RI index has an acceptably low error variance and is less susceptible to bias than any other RI anisotropy index proposed to date.

Key words: magnetic resonance imaging; anisotropy; diffusion; tensor.

INTRODUCTION

MR measurements of water diffusion in organs and tissues having an orderly, oriented structure, such as skeletal (1), cardiac (2), and uterine (3) muscle, portions of the kidney (4), the lens (5), and white matter (6–8), exhibit anisotropy (i.e., a dependence of the diffusivity on direction). The development of quantitative MRI measures of diffusion anisotropy could have important biological and clinical applications, helping physicians infer microstructural characteristics of normal tissues that are undetected by using other techniques, as well as pathological changes in tissue microstructure. This microstructural information may be useful in arriving at a correct diagnosis, as well as choosing and implementing appropriate therapies.

MRM 36:893–906 (1996)

From the Neuroimaging Branch, National Institute of Neurological Diseases and Stroke (NINDS) (C.P.), and the Biomedical Engineering and Instrumentation Program, NCRR (P.J.B.), The National Institutes of Health (NIH), Bethesda, Maryland.

Address correspondence to: Carlo Pierpaoli, M.D., NB/NINDS/NIH, Building 10, Room 1C227, 9000 Rockville Pike, Bethesda, MD 20892.

Received February 20, 1996; revised June 4, 1996; accepted June 19, 1996.

This work was performed in the *In Vivo* NMR Research Center, The National Institutes of Health (NIH), Bethesda, Maryland.

0740-3194/96 $3.00

However, while a qualitative indication of diffusion anisotropy can be obtained by inspecting diffusion-weighted images (DWIs), a quantitative assessment is more problematic as there are no universally agreed upon standards for measuring and reporting diffusion anisotropy, and there is no phantom that mimics the anisotropic diffusion properties of living tissues to which these MR measurements can be compared. On theoretical grounds, it has been predicted that currently used indices of diffusion anisotropy derived from DWIs or from two or three apparent diffusion coefficients (ADCs) measured in perpendicular directions are not quantitative. In particular, they are *rotationally variant* because their values depend on the direction of the applied diffusion gradients and the orientation of structures within each voxel (9). *Rotationally invariant* anisotropy measures, which have values that are independent of the laboratory frame of reference, of the direction of the applied diffusion gradients, and of the orientation of the tissue structures within each voxel, can be constructed from the diffusion tensor (**D**)(9–11).

The first goal of this paper was to assess the importance of rotational invariance on characterizing diffusion anisotropy *in vivo*. We used high-resolution DWIs of monkey brain to compute **D** on a voxel-by-voxel basis, and produce maps of both previously proposed rotationally variant anisotropy indices (12, 13) and recently developed rotationally invariant anisotropy indices (9, 14, 15). We then compared them in different anatomical regions of the brain. The second goal of this work was to examine the sensitivity of anisotropy measures to background noise inherent in all DWIs. This effect has not previously been accounted for or studied systematically, but it influences the mean and variance of all diffusion anisotropy measures estimated from DWIs. The level of confidence one has in a particular anisotropy measure clearly depends on its accuracy and precision. To analyze systematically the statistical properties of anisotropy indices for different levels of background noise and of diffusion anisotropy, we used synthetic diffusion data generated by using Monte Carlo methods. We used these simulations to help interpret our *in vivo* animal data. Finally, having examined the susceptibility to noise of previously proposed anisotropy measures, the third goal of this work was to identify a family of new invariant anisotropy indices with improved noise immunity.

METHODS

Animal Preparation

Six monkeys were studied under a protocol approved by the NINDS Animal Care and Use Committee. The preparation for the MR scan included sedation with ketamine (15 mg/kg administered intramuscularly), endotracheal

intubation, general anesthesia with Isoflurane, and surgical placement of catheters in both a femoral artery and a femoral vein. During the scan, the animals were anesthetized with 1.5% Isoflurane in 40% O_2 and 60% N_2O, mechanically ventilated, and immobilized with a constant intravenous infusion of succinylcholine chloride (6 to 10 mg/kg/h). The tidal volume was adjusted to produce PaO_2 of 130 mmHg or greater and $PaCO_2$ of 35 to 40 mmHg. Arterial blood pressure, heart rate, and expiratory CO_2 were monitored throughout the study. Arterial blood samples were withdrawn periodically for measurement of pH and blood gases. In a few studies in which the arterial catheter was not positioned, the heart rate was monitored by ECG. Body temperature was maintained at 37 ± 0.5°C by a circulating-water heating pad placed around the body.

MR Imaging

MR data were obtained with a General Electric 2T Omega MR system (GE NMR Instruments, Fremont, CA) with a horizontal bore with an inner diameter of 35 cm. The system included a self-shielded (Acustar 290) gradient set capable of producing gradient pulses up to 40 mTesla/m. A home-built quadrature coil (13-cm inner diameter) was used as a radio-frequency transmitter and receiver. The animal was centered in the magnet/gradient system with the aid of T_1-weighted MR images, and was not moved for the remainder of the study. The MR data were collected using a SE imaging sequence provided by the manufacturer (GE NMR Instruments, Fremont, CA) that was modified to acquire diffusion-weighted images. Imaging acquisition parameters were as follows: 4 coronal slices, 2 mm slice thickness, 256 × 128 in-plane resolution, 70 mm field of view, minimum *TR* of 2 s, cardiac gating on the first slice, *TE* of 70 ms, 2 repetitions per image. Diffusion sensitization was obtained by applying two symmetric diffusion gradient pulses before and after the 180° pulse (16–18). The trapezoidal diffusion gradients had a duration of 19.5 ms, a ramp time of 0.3 ms, and were separated by a time interval of 40 ms. Diffusion sensitizing gradients were applied sequentially along six different directions: {(0,0,1), (0,1,0), (1,0,0), (0,1/√2,1/√2), (1/√2,0,1/√2), and (1/√2, 1/√2,0)} using the following convention: x (phase encode, horizontal), y (readout, vertical), and z (slice select, bore). In each direction we acquired four images with peak diffusion gradient strengths of 7.5, 15, 22.5, and 30 mTesla/m. In total, 25 images were acquired, including one image with no diffusion sensitization.

Data Analysis

After Fourier magnitude reconstruction, the images were transferred to a SUN Sparc-10 and analyzed by using our software written in IDL (Iterative Data Language). For each image, the b-matrix was calculated from analytical expressions derived from the imaging and gradient waveforms (19). We estimated the six elements of the effective or apparent diffusion tensor, **D** (with independent components Dxx, Dyy, Dzz, Dxy, Dxz, and Dyz) and the signal intensity with no diffusion sensitization $A(\underline{b} = \mathbf{0})$; from the measured echo signal, $A(\underline{b})$ and each element of the calculated b-matrix, b_{ij}, by using (11):

$$\mathrm{Ln}\left(\frac{A(\underline{b})}{A(\underline{b}=0)}\right) = -\sum_{i=1}^{3}\sum_{j=1}^{3} b_{ij}D_{ij} \qquad [1]$$

The apparent diffusion coefficients (ADCs) one obtains by applying diffusion gradients along the x, y, and z coordinate directions (ADCx, ADCy, and ADCz, respectively) equal the diagonal elements of the diffusion tensor above (Dxx, Dyy, and Dzz), when there are no contributions of imaging gradients to the b-values used to calculate these ADCs. Since, in our experiment, these "cross-terms" were not negligible, we use the diagonal elements of the diffusion tensor as proxies for the ADCs when computing all anisotropy indices that employ them.

Background noise levels used to estimate the experimental error variances in the linear regression routine were obtained by measuring the root-mean-squared (r.m.s.) signal intensity in regions of the images containing no tissue. We set the weighting factor of the linear regression algorithm to be the square of the r.m.s. background noise in each image divided by the square of the signal intensity in each voxel. This was done to correct the bias in the experimental variance introduced by taking the logarithm of the measured amplitude signal (20). This method, however, does not correct for the distortion produced by taking the logarithm of the rectified noise when the signal is very low.

Monte Carlo Simulations

Monte Carlo simulations were performed to assess the effect of noise on the various anisotropy indices estimated from the diffusion tensor. We started with diffusion tensors whose trace is representative of brain parenchyma (2100×10^{-6} mm^2/s), but with different degrees of diffusion anisotropy. For simplicity, we assumed the anisotropic tissue's principal axes coincided with the laboratory frame of reference. We also limited our investigation to the case of cylindrically symmetric diffusion anisotropy. By using the same set of 25 b-matrices that we used in the animal experiments, we generated 25 synthetic, noise-free DW signal intensities by using Eq. [1] above. We then simulated thermal noise in the MR measurement. First, we generated complex random numbers whose real and imaginary parts were Gaussian distributed with mean of 0 and standard deviation scaled to the desired r.m.s. noise level. Then we added the noise-free signal to the real part of the complex noise, and took the magnitude of this complex number to generate the noisy amplitude signal. To check the validity of this approach, we showed that the standard deviation of the noisy amplitude signal equaled the selected r.m.s. noise level (21). For each assumed diffusion tensor, 16,384 replicates were performed.

Definition of the Anisotropy Indices

Here we present definitions of diffusion anisotropy measures used in our imaging and simulation studies, and a

brief description of their properties. A thorough review of diffusion anisotropy measures used to date has been presented elsewhere (22).

Rotationally Variant Anisotropy Indices. Most published clinical and animal studies that treat diffusion anisotropy have employed rotationally variant indices. The most widely used is the one proposed by Douek *et al.* (12), which is defined as the *ratio of two apparent diffusion-coefficients*, with diffusion sensitizing gradients applied in two perpendicular directions. In this paper, we do not explicitly calculate rotationally variant two-dimensional anisotropy indices but, for each region of interest, we do present the values of the ADCs in the x, y, and z directions from which such indices can be calculated. Moreover, we compare the three ADCs and the three eigenvalues of **D** (Table 2).

More recently, rotationally variant anisotropy indices that employ three ADCs measured in three mutually perpendicular directions have been proposed (13, 23). A three-dimensional anisotropy index potentially provides a succinct description of anisotropy by a single scalar quantity. One index that has already been used to map anisotropy of the human brain (24) is the *standard deviation index* (SD) proposed by van Gelderen *et al.* (13). SD is a scalar anisotropy index that is proportional to the standard deviation of three ADCs measured in mutually perpendicular directions: ADCx, ADCy, and ADCz, divided by their mean value, <ADC>. Another three-dimensional, rotationally variant scalar anisotropy index, which we define here and use only for comparison with its invariant analog, is the *rotationally variant Volume Ratio index* (RV Volume Ratio). The RV Volume Ratio index is computed from the Volume Ratio index shown below by substituting the ADCs in three mutually perpendicular directions for the eigenvalues of the diffusion tensor.

Rotationally Invariant Anisotropy Indices. When a diffusion tensor is diagonalized, we obtain its eigenvectors and eigenvalues. The eigenvectors of **D** represent the three mutually perpendicular directions along which molecular displacements of the spin-labeled molecules appear uncorrelated, while the eigenvalues of **D** are the diffusivities along these preferred directions. We can sort the eigenvalues of **D** in order of decreasing magnitude (λ_1 = highest diffusivity, λ_2 = intermediate diffusivity, and λ_3 = lowest diffusivity). In anisotropic tissues organized in parallel bundles, the largest eigenvalue, λ_1, represents the diffusion coefficient in the direction parallel to the fibers ($D_{\|}$) in each voxel, while λ_2 and λ_3 are the transverse diffusion coefficients ($D\perp$ and $D\perp'$). The most intuitive and simplest rotationally invariant indices are *ratios of the principal diffusivities* (9), such as the dimensionless anisotropy ratio λ_1/λ_3 that measures the relative magnitudes of the diffusivities along the fiber-tract direction and one transverse direction. In this paper, we analyze the behavior of λ_1/λ_3 and $\lambda_1/(\lambda_2 + \lambda_3)/2$.

While calculating the ratios of the principal diffusivities requires us to sort the eigenvalues according to their magnitude, other invariant anisotropy indices can be constructed so that they are independent of the way we order the eigenvalues. One such index is the *Volume Ratio* (14):

$$\text{Volume Ratio} = \frac{\lambda_1\lambda_2\lambda_3}{\left(\frac{\lambda_1 + \lambda_2 + \lambda_3}{3}\right)^3} = 27\,\frac{\text{Determinant}(\mathbf{D})}{\text{Trace}(\mathbf{D})^3} \qquad [2]$$

The Volume Ratio has a simple geometrical interpretation; it represents the volume of an ellipsoid whose semi-major axes are the three eigenvalues of (**D**) divided by the volume of a sphere whose radius is the mean diffusivity, Trace(**D**)/3. Since the volume of the ellipsoid approaches 0 as anisotropy increases, the values of Volume Ratio range between 0 and 1, where 0 indicates the highest anisotropy and 1 represents complete isotropy. The right hand side of the equation shows that this index is the ratio of two scalar invariant quantities computed from the diffusion tensor, its Determinant and its Trace, thus assuring rotational invariance.

Recently, other invariant measures of diffusion anisotropy have been proposed that do not require sorting of the eigenvalues (15). They employ the tensor dot product of the *anisotropic part* of the diffusion tensor $\boldsymbol{D}$ with itself, $\boldsymbol{D} : \boldsymbol{D}$, as a scalar measure of the magnitude of diffusion anisotropy in a voxel. (Note that **D** (bold, no italics) represents the diffusion tensor itself, while $\boldsymbol{D}$ (bold, italicized) represents only its anisotropic part or the diffusion deviatoric.) We analyze the statistical behavior of two of them: the *relative anisotropy* (RA) (15) and the *fractional anisotropy* (FA) (15).

"Lattice" Anisotropy Index

The eigenvalues of **D** represent only three of the seven parameters estimated from the data set of diffusion-weighted images. The other parameters are the T_2-weighted signal intensity in the absence of diffusion sensitization (A(0)), and three parameters containing orientational information (e.g., Euler angles) that can be used to specify the eigenvectors of **D**. Diffusion anisotropy is intrinsically related to the eigenvalues, which determine the shape of the diffusion ellipsoids, not to their eigenvectors, which specify their orientation. Therefore, it is sensible that the rotationally invariant "intravoxel" anisotropy indices proposed to date do not contain the eigenvectors of **D**. Nevertheless, since noise affects diffusion measurements, it is both reasonable and desirable to use the remaining estimated parameters to improve our estimate of the diffusion anisotropy in each voxel.

How can we use the directional information contained in the diffusion tensor to reduce the noise of our anisotropy measure? Consider a voxel where the diffusion process is isotropic and where differences in the estimated eigenvalues of **D** result solely from random noise. If we were to perform many replicate experiments, we would expect the eigenvectors of **D** in that particular voxel to be uncorrelated, and the principal axes of the corresponding diffusion ellipsoids to be random. Moreover, the orientation of the diffusion ellipsoid in one voxel should be uncorrelated with that of its neighbors. By contrast, if the

tissue were anisotropic, the diffusion ellipsoid in a particular voxel would have a preferred direction, and, would therefore be correlated with the orientation of the ellipsoids in adjacent voxels.

To improve our estimate of diffusion anisotropy in a particular voxel, we propose using an anisotropy index that is affected by the degree of orientational coherence of the diffusion ellipsoid in the reference voxel with those in neighboring voxels. This requires a means to measure the degree of collinearity of the eigenvectors of **D** in different voxels. A natural measure is the square of the cosine of the angle between eigenvectors, which is obtained by taking the square of the dot products between the two eigenvectors ϵ and ϵ'. However, a more general and geometrically satisfying approach is to use a measure of collinearity that weights each eigenvector by the corresponding principal diffusivity or eigenvalue. By summing the squares of the vector dot product between each pair of semi-major axes, $\sqrt{\lambda_s}\epsilon_s$, and $\sqrt{\lambda'_k}\epsilon'_k$, respectively, we obtain:

$$\mathbf{D} : \mathbf{D}' = \sum_{k=1}^{3} \sum_{s=1}^{3} (\sqrt{\lambda_s}\epsilon_s \cdot \sqrt{\lambda'_k}\epsilon'_k)^2 \qquad [3]$$

where k and s are indices that run from 1 to 3. Previously, we proposed the quantity $\mathbf{D} : \mathbf{D}'$ as a measure of structural (diffusive) similarity between media in two different voxels with diffusion tensors **D** and **D'**. $\mathbf{D} : \mathbf{D}'$ also possesses the required properties of a quantitative measure (i.e., objectivity as well as rotational invariance) (15). For given values of Trace(**D**) and Trace(**D'**), $\mathbf{D} : \mathbf{D}'$ is maximized when the corresponding eigenvectors of **D** and **D'** are collinear.

We can now form the tensor dot product between the anisotropic parts of diffusion tensors in different voxels, $\boldsymbol{D} : \boldsymbol{D}'$, which can be written as

$$\boldsymbol{D} : \boldsymbol{D}' = \mathbf{D} : \mathbf{D}' - \frac{1}{3}\,\mathrm{Trace}(\mathbf{D})\,\mathrm{Trace}(\mathbf{D}') \qquad [4]$$

Just as the tensor dot product of the anisotropic part of the diffusion tensor $\boldsymbol{D}$ with itself, $\boldsymbol{D} : \boldsymbol{D}$, provides an *intravoxel* scalar measure of the magnitude of diffusion anisotropy, the tensor dot product between the anisotropic parts of diffusion tensors in different voxels, $\boldsymbol{D} : \boldsymbol{D}'$, could be used as a basis for the definition of a family of *intervoxel* or "lattice" scalar measures of diffusion anisotropy. In this paper, we present one of those measures with a particularly good dynamic range for different levels of diffusion anisotropy and a small bias.

If we take $\mathbf{D}_{\mathrm{ref}}$ and $\boldsymbol{D}_{\mathrm{ref}}$ to be, respectively, the diffusion tensor and its deviatoric in a reference voxel, and $\mathbf{D}_{\mathrm{N}}$ and $\boldsymbol{D}_{\mathrm{N}}$ to be the diffusion tensor and its deviatoric in an arbitrary (neighboring) voxel, the basic element of the lattice index (LI_{N}) is defined as:

$$\mathrm{LI}_{\mathrm{N}} = \frac{\sqrt{3}}{\sqrt{8}}\left(\frac{\sqrt{\boldsymbol{D}_{\mathrm{ref}} : \boldsymbol{D}_{\mathrm{N}}}}{\sqrt{\mathbf{D}_{\mathrm{ref}} : \mathbf{D}_{\mathrm{N}}}} + \frac{\sqrt{\boldsymbol{D}_{\mathrm{ref}} : \boldsymbol{D}_{\mathrm{N}}}\,\sqrt{\boldsymbol{D}_{\mathrm{ref}} : \boldsymbol{D}_{\mathrm{N}}}}{\mathbf{D}_{\mathrm{ref}} : \mathbf{D}_{\mathrm{ref}}}\right) \qquad [5]$$

We can obtain a local *intervoxel* anisotropy index by averaging this quantity over a region of interest (ROI). Although there are many ways to compute this average within each slice, one simple approach is to choose an ROI that includes only the eight voxels that are contiguous to the reference voxel, weighting their contributions according to their distance from the reference voxels:

$$\mathrm{LI}_{\mathrm{ref}} = \sum_{N=1}^{8} a_N \mathrm{LI}_N \Big/ \sum_{N=1}^{8} a_N \qquad [6]$$

where $\mathrm{LI}_{\mathrm{ref}}$ is the "lattice" index in the reference voxel, and "a" is a weighting factor whose value is 1 for voxels that share a side with the reference voxel and $1/\sqrt{2}$ for voxels that share only a vertex with the reference voxel.

The computer program we used to calculate the lattice index from the elements of the diffusion tensor is available upon request. The code is written in IDL (Iterative Data Language).

RESULTS

Figure 1 shows a diffusion ellipsoid image (coronal section) of a region of monkey brain. The diffusion ellipsoids are surfaces of constant mean-squared displacement of diffusing water molecules at some time τ after they are released at the center of each voxel. This image is presented to underscore how the diffusion ellipsoids summarize the information contained in the diffusion tensor. The degree of diffusion anisotropy is embodied in the shape or eccentricity of the diffusion ellipsoid; the bulk mobility of the diffusing species is related to the size of the diffusion ellipsoid; and the preferred directions of diffusion are indicated by the orientation of the diffusion ellipsoid. If the tissue were isotropic, then the water mobility would be the same in all directions, and these surfaces would be spherical. However, if the medium

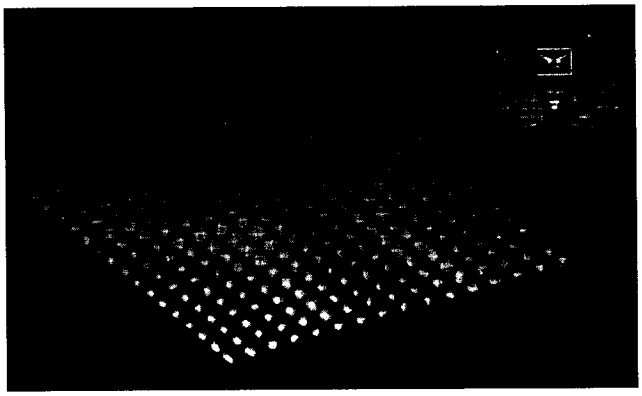

FIG. 1. Diffusion ellipsoid image of monkey brain. Diffusion ellipsoids represent surfaces of constant mean-squared translational displacement some time τ after the spin-labeled molecule is released at a point at the center of a voxel. They are calculated in each voxel of the ROI enclosed by the rectangle shown on the T_2-weighted image. The shape of the diffusion ellipsoid is intrinsically related to the diffusion anisotropy and can be characterized by using the three scalar principal diffusivities: The largest diffusivity, λ_1, is the mobility of water in the direction parallel to the fibers (D$\|$), while λ_2 (D$\perp$) and λ_3 (D$\perp'$) are the two transverse diffusivities perpendicular to the fiber direction.

were anisotropic, like brain white matter, then the mobility would depend on the direction in which it is measured, and these surfaces would be ellipsoidal. Examples of both anisotropic white matter and isotropic gray matter can be found in Fig. 1. In isotropic media like gray matter and the CSF-filled ventricles, ellipsoids are spherical. However, since water diffusivity is lower in gray matter than in free water, the size of the ellipsoid in gray matter is smaller than in CSF. In white matter, the ellipsoids are more elongated than in gray matter. Although the diffusion ellipsoids embody the information contained in the diffusion tensor, they provide a useful pictorial representation of diffusion anisotropy, but not a quantitative description of it.

Table 1 shows the x, y, and z components of the applied diffusion gradients, Gx, Gy, and Gz, for one non-diffusion-weighted image and for the six most heavily weighted-diffusion images. The associated b-matrix elements computed from each DWI gradient sequence are also shown. The effects of cross-terms (i.e., interactions between diffusion and imaging gradients) are most pronounced in the read-out (y) direction. When Gx = 30 mTesla/m and all other diffusion gradients are zero, bxx = 830.5 s/mm^2; when Gy = 30 mTesla/m and all other diffusion gradients are zero, byy = 974.6 s/mm^2. This disparity is due to the read-out pre-dephase gradient applied at the beginning of the sequence, just after the 90° pulse. When diffusion gradients are applied along two directions simultaneously, such as along x and y (in line 5) or x and z (in line 6), we see a lack of symmetry in the off-diagonal elements, bxy and bxz, which is also caused by imaging gradients.

Figure 2 shows images of Dxx, Dyy, and Dzz (which are proxies for the respective ADCs measured along the x, y, and z coordinate directions: ADCx, ADCy, and ADCz). Variations in the relative contrast in most of the white matter fiber tracts suggest diffusion anisotropy. These images also indicate the direction along which the diffusion sensitizing gradients are applied. In contrast, the three images of the eigenvalues of **D** (principal diffusivities), λ_1, λ_2, and λ_3, sorted in order of decreasing size, display features that are intrinsic to the tissue, but are independent of the direction of the diffusion sensitizing gradients used to acquire the diffusion-weighted images. Accompanying Fig. 2 is Table 2, containing values of the diagonal elements of **D** (Dxx, Dyy, and Dzz) juxtaposed with the eigenvalues of **D** (λ_1, λ_2, and λ_3) computed in different anatomical regions of interest in the monkey brain. The sorted eigenvalues of **D** suggest that water diffusion is highly anisotropic in white matter, where the values of λ_1 (range: 1400–1800 × 10^{-6} mm^2/s) are much larger than the values of λ_2 (360–460 × 10^{-6} mm^2/s) and λ_3 (140–240 × 10^{-6} mm^2/s). The optic tract shows the highest values of λ_1, followed by the corpus callosum and internal capsule. Regions having the highest λ_1 also tend to have the lowest values of λ_2 and λ_3. Statistically significant differences exist between λ_1 and λ_2, as well as between λ_2 and λ_3, in all regions. In general, the diagonal elements of **D** are significantly different from the eigenvalues. However, this discrepancy is more pronounced in some anatomical regions than in others. For example, in the corpus callosum, the diagonal elements and the eigenvalues of **D** are similar, whereas in the internal capsule they are different. While the distribution of the eigenvalues is similar in the corpus callosum and the anterior internal capsule, suggesting high anisotropy in both regions, the distribution of the diagonal elements of the diffusion tensor is not, suggesting high anisotropy in the corpus callosum but complete isotropy in the anterior internal capsule. Similar results are observed in Table 3 and Fig. 3 comparing rotationally invariant anisotropy indices calculated from the eigenvalues of **D**, and their rotationally variant counterparts, constructed from the diagonal elements of **D**. As previously reported (13), Trace(**D**) appears to be relatively homogeneous throughout the brain.

Figure 4 shows the estimated means and standard deviations of principal diffusivities, λ_1, λ_2, and λ_3, as functions of the signal-to-noise-ratio (SNR) of the non-diffusion-weighted data. Data in Fig. 4a are generated by a Monte Carlo simulation, assuming a diffusion tensor representative of isotropic tissue (comparable with gray matter). Asymptotic values (i.e., those with infinite SNRs) are $\lambda_1 = \lambda_2 = \lambda_3 = 700 \times 10^{-6}$ mm^2/s. For any non-zero noise level, there is a significant difference between the true and the simulated values of λ_1 and λ_3. Inherently, λ_1 is larger than its asymptotic value and λ_3 is smaller than its asymptotic value. The bias in the value of λ_2 is much smaller for all SNRs. An additional bias (introduced by the logarithmic transformation used to estimate diffusion tensor elements) becomes significant only when SNR drops below 10. Figure 4b shows results of a simulation in cylindrically symmetric anisotropic tissue with principal diffusivities comparable with those of a highly

Table 1
Components of the Applied Diffusion Gradients for One Image with no Diffusion Weighting and the Six Most Heavily Diffusion-Weighted Images, along with Their Corresponding b-Matrix Values

Diffusion gradients (mTesla/m)			B-Matrix (s/mm^2)					
Gx	Gy	Gz	bxx	byy	bzz	2*bxz	2*bxy	2*byz
0.0	0.0	0.0	0.1	8.3	0.3	0.3	−0.9	−1.2
30.0	0.0	0.0	830.5	8.3	0.3	12.9	−146.9	−1.2
0.0	30.0	0.0	0.1	974.6	0.3	0.3	−11.0	−13.8
0.0	0.0	30.0	0.1	8.3	833.2	10.4	−0.9	−147.1
21.2	21.2	0.0	448.7	556.5	0.3	9.5	−997.7	−10.5
21.2	0.0	21.2	448.7	8.3	450.7	899.3	−107.9	−108.2
0.0	21.2	21.2	0.1	556.5	450.7	7.7	−8.3	−999.8

While the imaging gradients contribute negligibly to the b-matrix with no diffusion sensitization, their contribution is significant with maximal diffusion sensitization.

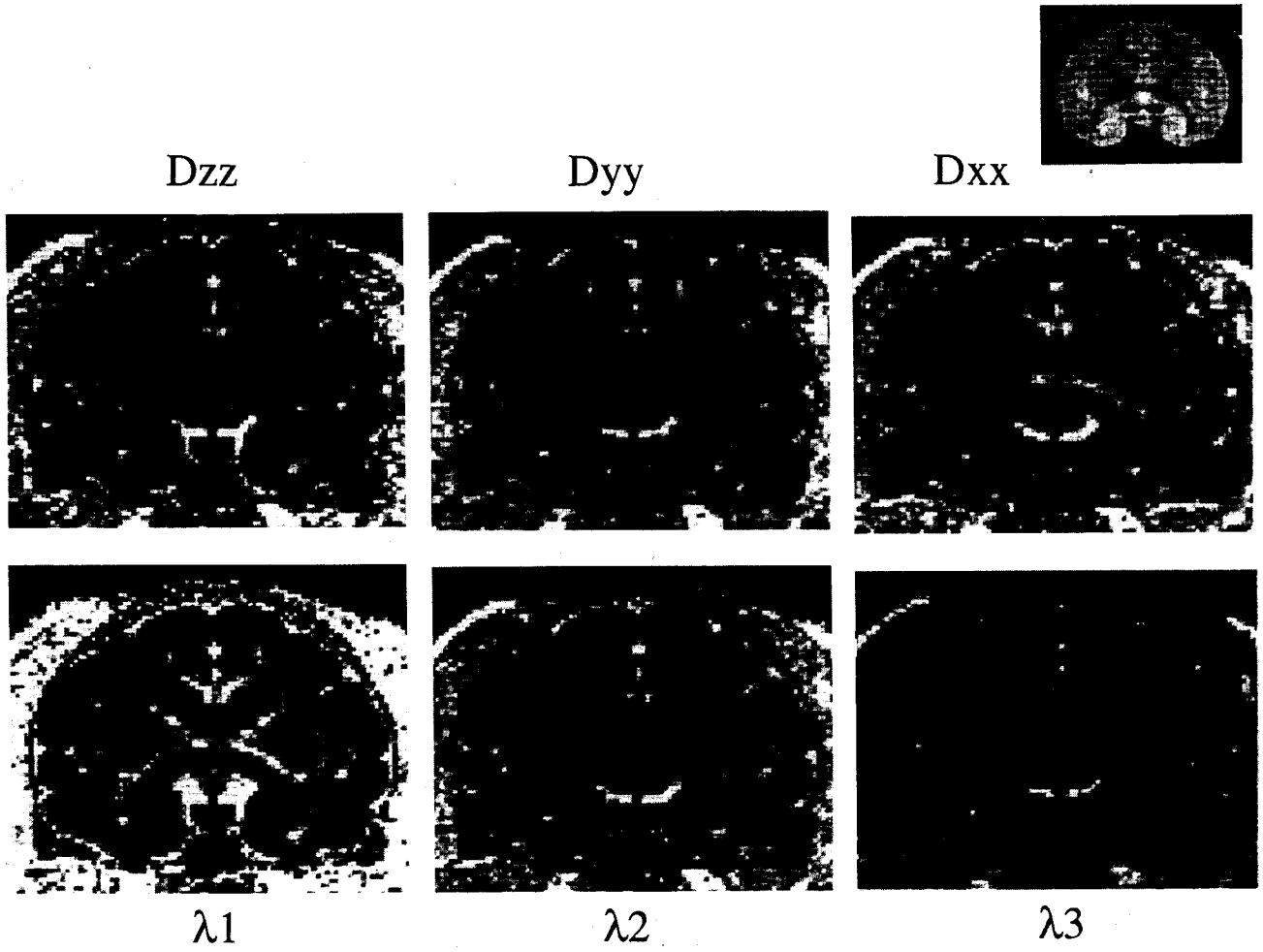

FIG. 2. Maps of quantities calculated from **D** in each voxel in a coronal section of monkey brain. Top insert on the right shows the T_2-weighted amplitude image (A(b = 0)). Top row contains three images showing the diagonal elements of **D**: Dxx, Dyy, and Dzz. Bottom row contains three images showing the eigenvalues of **D** (principal diffusivities): λ_1, λ_2, and λ_3, sorted in order of decreasing size.

anisotropic white matter tract ($\lambda_1 = 1500 \times 10^{-6}$ mm^2/s, $\lambda_2 = \lambda_3 = 200 \times 10^{-6}$ mm^2/s). In this case, λ_2 is systematically larger than its asymptotic value and λ_3 is smaller than its asymptotic value. For very low SNR levels, negative values of λ_3 can be observed. While this is physically impossible, we do not explicitly constrain the eigenvalues of **D** to be positive when we estimate them. The value of λ_1 is relatively unbiased for all SNRs in white matter-like tissue.

In Fig. 5, the Monte Carlo simulated data are used to construct different invariant anisotropy indices, as a function of SNR, for levels of anisotropy in the range of

Table 2
Diagonal Elements of the Diffusion Tensor, Dxx, Dyy, and Dzz Are Compared with the Sorted Principal Diffusivities (Eigenvalues of **D**), λ_1, λ_2, and λ_3, in Different Anatomical Regions of the Monkey Brain

	Corpus callosum	Optic tract	Posterior internal capsule	Anterior internal capsule	Subcortical white matter	Putamen	Caudate	Parietal cortex
D XX	1481 ± 93	1064 ± 122	511 ± 72	678 ± 69	780 ± 119	690 ± 52	683 ± 49	669 ± 48
D YY	431 ± 54	267 ± 91	1170 ± 125	660 ± 77	727 ± 89	677 ± 56	695 ± 57	727 ± 83
D ZZ	330 ± 87	1004 ± 106	423 ± 174	856 ± 99	501 ± 119	699 ± 87	751 ± 85	664 ± 82
λ1	1690 ± 92	1863 ± 105	1487 ± 85	1483 ± 107	1019 ± 64	861 ± 94	890 ± 70	921 ± 68
λ2	389 ± 71	360 ± 77	453 ± 68	467 ± 44	658 ± 51	684 ± 53	704 ± 53	655 ± 50
λ3	181 ± 44	140 ± 31	183 ± 49	246 ± 30	334 ± 76	521 ± 61	535 ± 75	484 ± 62
Trace	2242 ± 175	2335 ± 143	2105 ± 204	2194 ± 156	2009 ± 145	2066 ± 180	2129 ± 169	2059 ± 156

Dxx, Dyy, and Dzz are proxies of the ADCx, ADCy, and ADCz, obtained by applying diffusion gradients in the x, y, and z directions, respectively. All values have been calculated on a voxel-by-voxel basis and then averaged within the ROI. For bilateral structures, measurements from left and right regions have been pooled. Average values (μ^2/s) ±SD of measurements made in six animals are presented.

Table 3
A Comparison between Rotationally Invariant Anisotropy Indices (e.g., Volume Ratio, Relative Anisotropy) and Their Respective Rotationally Variant (RV) Analogues (RV Volume Ratio and SD)

	Corpus callosum	Optic tract	Posterior internal capsule	Anterior internal capsule	Subcortical white matter	Putamen	Caudate	Parietal cortex
1-Volume Ratio	0.74 ± 0.06	0.81 ± 0.05	0.68 ± 0.06	0.58 ± 0.04	0.30 ± 0.11	0.08 ± 0.04	0.08 ± 0.05	0.12 ± 0.04
1-Volume Ratio (rotationally variant)	0.55 ± 0.09	0.48 ± 0.13	0.40 ± 0.15	0.07 ± 0.03	0.13 ± 0.09	0.01 ± 0.00	0.02 ± 0.01	0.03 ± 0.02
Relative anisotropy	0.65 ± 0.05	0.71 ± 0.06	0.59 ± 0.07	0.52 ± 0.03	0.31 ± 0.06	0.15 ± 0.04	0.15 ± 0.04	0.19 ± 0.03
SD (rotationally variant)	0.51 ± 0.06	0.37 ± 0.05	0.39 ± 0.09	0.13 ± 0.03	0.19 ± 0.07	0.06 ± 0.01	0.06 ± 0.02	0.09 ± 0.03

The rotationally invariant anisotropy indices are constructed from the principal diffusivities, while the rotationally variant indices are constructed using ADCs with diffusion gradients applied in three perpendicular directions. The rotationally invariant indices show a degree of anisotropy that is systematically larger than their rotationally variant counterparts, however, the disparity between them is markedly smaller in structures that are approximately parallel or perpendicular to the laboratory axes (like the corpus callosum), and larger for structures that are oblique with respect to the three laboratory axes (like the anterior internal capsule).

those observed in brain tissue. The systematic bias, while individually making λ_1 larger and λ_3 smaller than their true values, causes their ratio, λ_1/λ_3, to be significantly larger than its true value at all noise levels (Fig. 5a). In addition, the variance of this ratio is significantly larger in anisotropic media than in isotropic media. In Fig. 5b, we see that the bias is much less pronounced than in Fig. 5a, in particular for high values of anisotropy, and the predictions are more reliable over a larger range of SNRs. The Volume Ratio (Fig. 5c), and the Fractional Anisotropy (Fig. 5d), are two intravoxel anisotropy indices that are insensitive to sorting of the eigenvalues. They exhibit a lower variance at all SNRs than the anisotropy ratio. Moreover, this variance is less sensitive to differences in anisotropy among tissues. Still, they exhibit a significant bias, resulting in a progressive increase in anisotropy as SNR decreases. The "lattice" anisotropy index (Fig. 5e) shows the lowest bias and variance.

Finally, Fig. 6 contains images showing the T_2-weighted amplitude, A(0), the Lattice Anisotropy index,

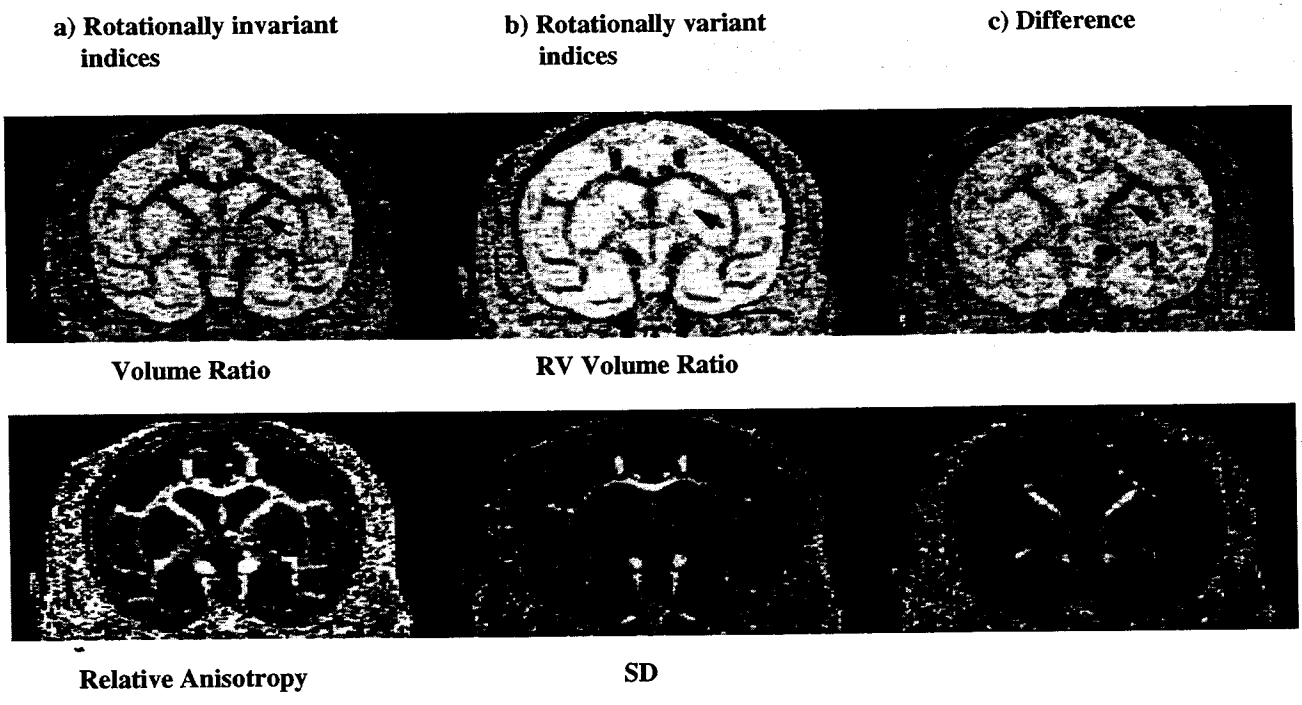

FIG. 3. A comparison between maps of rotationally invariant and rotationally variant anisotropy indices in a coronal section of monkey brain: (a) the rotationally invariant Volume Ratio (top) and Relative Anisotropy (bottom) indices; (b) the corresponding rotationally variant analogs, RV Volume Ratio and SD; and (c) the absolute value of their difference. The possible values of Volume Ratio lie between 0 and 1, where 0 indicates the highest anisotropy (dark) and 1 represents complete isotropy (bright). Arrows point to the internal capsule, a structure that appears to be as isotropic as gray matter in the images of the rotationally variant indices. The rotationally invariant indices, however, are prone to a noise-induced bias that makes regions where the signal is low appear more anisotropic than they are. This effect is particularly evident in the muscles surrounding the skull.

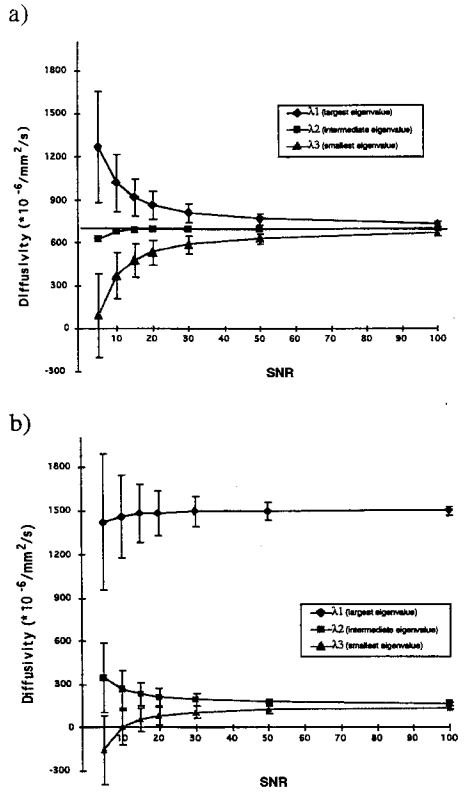

FIG. 4. The distribution of the sorted principal diffusivities, λ_1, λ_2, and λ_3 (generated by Monte Carlo simulations), as a function of the signal-to-noise ratio (SNR). Mean values ± standard deviation of 16,328 replicates are shown for a voxel containing (a) isotropic tissue and (b) anisotropic tissue. In the isotropic case, the standard deviation of λ_2 is not displayed to make the figure more legible.

and the Trace of the diffusion tensor, Trace(**D**), in different coronal sections of the monkey brain.

DISCUSSION

In this paper, we evaluate various factors that should be taken into consideration to measure diffusion anisotropy of living tissues quantitatively. First, we ensure that the b-matrix is correctly calculated. The contribution of cross-terms arising from imaging and diffusion gradients has been extensively described previously (19, 25, 26) and will not be discussed here. For our sequence, the contributions of the imaging gradients to the b-matrix were significant, and we had to take them into account by computing the b-matrix from the entire gradient pulse sequence (19). However, failing to account for imaging gradients in estimating the diffusion tensor is not the primary source of error in quantitating diffusion anisotropy. Although in this study we would have made a 17% error in the estimated diffusion tensor elements by ignoring imaging gradients, this is dwarfed by the error one makes in using a rotationally variant anisotropy index to characterize diffusion anisotropy in white matter, as described in the next section. Moreover, as suggested by Le Bihan (26), the contribution of the imaging gradients can be mitigated by refocusing the imaging gradients as soon as possible after they are applied. This principle has been implemented successfully in designing new sequences for use in clinical studies (27, 28).

Rotational Invariance

As stated earlier, invariant anisotropy indices cannot be calculated by using ADCs acquired in only two or three perpendicular directions. In general, it is necessary to determine the three eigenvalues of **D**, which can be calculated from the six estimated diffusion tensor elements. This requirement highlights an important difference between characterizing diffusion anisotropy and measuring the average diffusivity (or Trace(**D**)): The latter can be calculated from ADCs acquired in three perpendicular directions (when imaging gradients are negligible), whereas the former cannot.

The first goal of this paper was to assess the importance of rotational invariance on characterizing diffusion anisotropy *in vivo*. This is significant because, to date, diffusion anisotropy *in vivo* has only been reported using rotationally variant anisotropy indices. Therefore, one's level of confidence in these previous studies must be related to the severity of the errors caused by using these indices of diffusion anisotropy. Moreover, if it were found that one could measure diffusion anisotropy adequately by using a rotationally variant index (e.g., calculated from three perpendicular ADCs), then it would not be necessary to estimate the full diffusion tensor to characterize diffusion anisotropy, thus reducing the number of acquisitions and simplifying the analysis of DWIs significantly.

Using Table 2, Table 3, and Fig. 3, we can now address these issues. Our data show that in white matter, the range of the diagonal elements of the diffusion tensor (proxy of the ADCs) is consistently smaller than the range of the principal diffusivities. Moreover, rotationally variant anisotropy indices consistently show a lower degree of anisotropy than their invariant analogs. As expected, however, the magnitude of this difference depends on the relative orientation of the fiber tracts with respect to the x-y-z laboratory coordinate directions. In general, it is small but significant in structures that lie approximately parallel to one of the laboratory coordinate axes (like the corpus callosum), and it is large in structures that lie oblique to the three laboratory axes (like the anterior internal capsule). This phenomenon is clearly seen in Fig. 3, in which images of the rotationally invariant indices (Volume Ratio and RA) and their respective rotationally variant analogs (RV Volume Ratio and SD) are juxtaposed. In the internal capsule, the degree of diffusion anisotropy as measured by the rotationally variant indices is so low that this highly anisotropic structure appears indistinguishable from the surrounding isotropic gray matter.

There is an insidious character to this orientational artifact. While skewness between the fiber-tract direction and the laboratory axes is very evident when it occurs in the plane of the image (such as in the internal capsule in our images), it is more difficult to observe when it occurs in a plane perpendicular to the image plane (such as in the optic tract in our images). In the optic tract one might

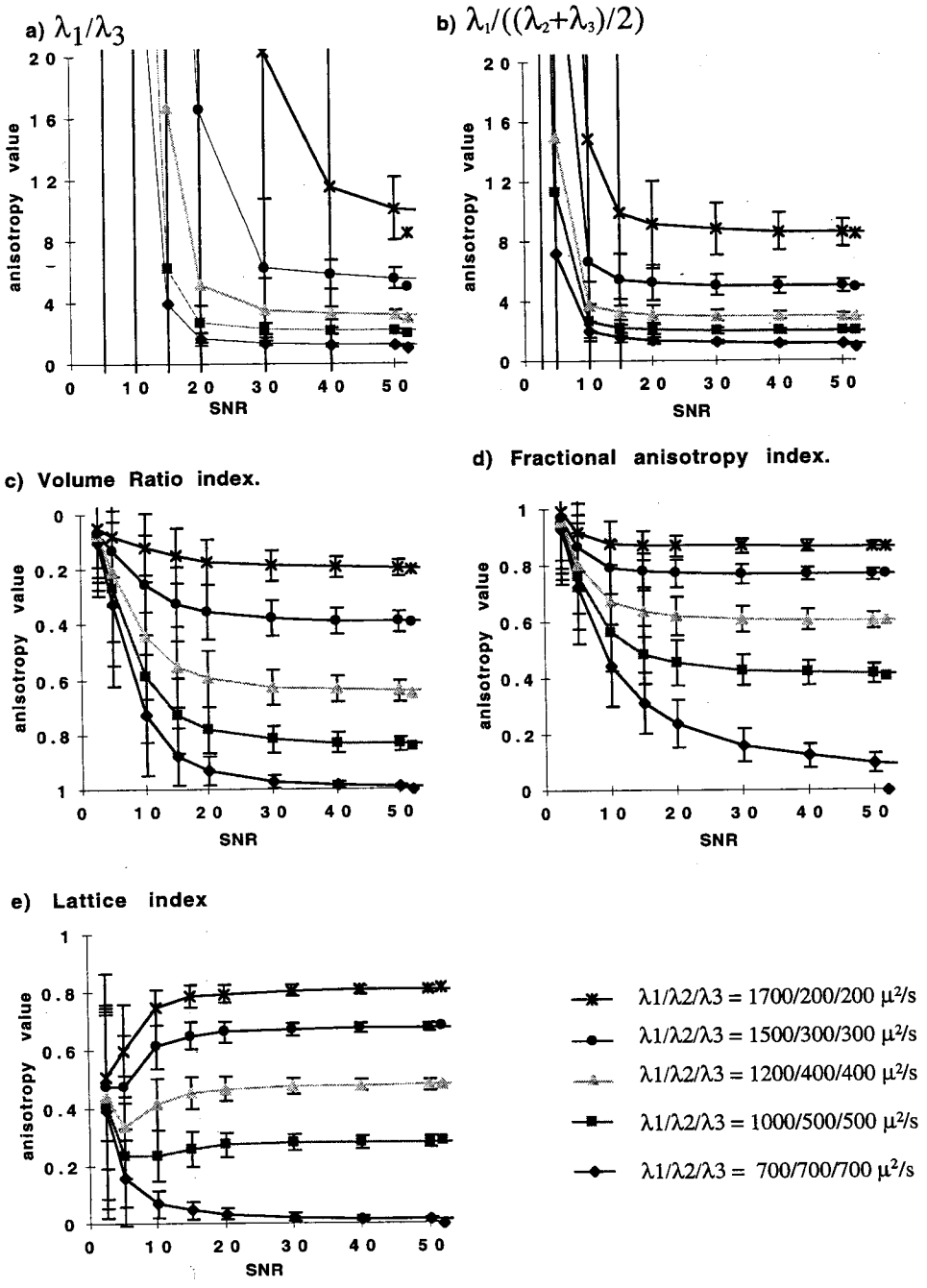

FIG. 5. Simulated values of rotationally invariant anisotropy indices as a function of the signal-to-noise ratio (SNR) generated by Monte Carlo methods. Each simulation consists of 16,328 replicates. For each index, a simulation is performed with five different levels of diffusion anisotropy, spanning the range of eigenvalues we observe in brain tissue. Cylindrical symmetry of diffusion is assumed ($\lambda_2 = \lambda_3$). Mean value ± standard deviation are shown for the (a) anisotropy ratio index λ_1/λ_3, (b) anisotropy ratio index $\lambda_1/(\lambda_2 + \lambda_3)/2$, (c) Volume Ratio index, (d) Fractional Anisotropy index, and (e) "Lattice" Anisotropy index. Since for the Volume Ratio, 1 represents complete isotropy and 0 indicates the highest anisotropy, for this index the scale of the y-axis is inverted. For all plots, values of SNR up to 50 are presented. The last point on the right of each curve indicates the true value of the index (i.e., for an infinite SNR).

think that the fibers run anterior to posterior, perpendicular to the x-y image plane; notwithstanding, the significant differences between the diagonal elements of the tensor and the principal diffusivities indicate that the trajectory of these fibers is actually oblique to the z axis. By using a rotationally variant anisotropy measure, we would significantly underestimate the anisotropy of the optic tract, the most anisotropic structure we investigated in this study.

The orientational artifact introduced by rotationally variant measures would not be problematic if we could always orient the tissue in the magnet such that we could apply diffusion gradients precisely along the principal directions of the structures of interest. However, in most clinical and experimental *in vivo* MRI applications, this is impossible. Even if we could properly align the diffusion gradients with the principal axes of the tissue in one voxel, we are virtually assured that these gradients will not coincide with the principal axes of tissues in other voxels, because the anisotropic tissues of interest exhibit a non-uniform fiber direction field. This is clearly evident in brain white matter. Even if the fiber directions were more uniform and homogeneous, we still recommended performing tests to establish a correspondence between the purported fiber tract direction and that which is measured from the diffusion tensor data.

We must conclude that rotational invariance is a necessary property of a quantitative measure of diffusion

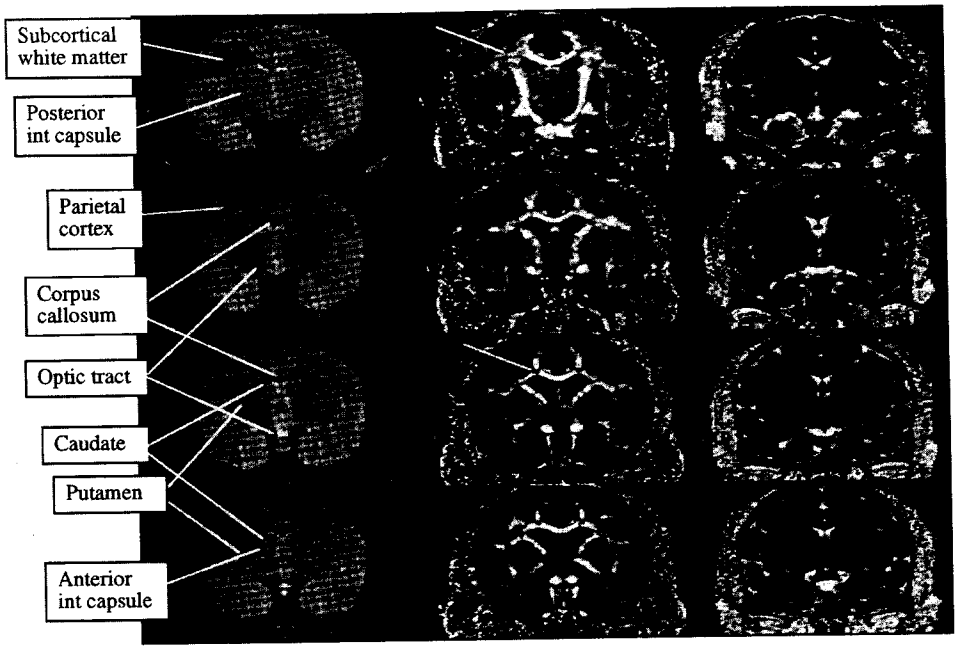

FIG. 6. Coronal images of monkey brain showing (a) the T_2-weighted amplitude, A(b = 0), (b) the "Lattice" anisotropy index, and (c) the Trace of the diffusion tensor, Trace(**D**). On the amplitude image, arrows point to the region selected for ROI analysis; on the "Lattice" anisotropy index image, arrows point to white matter regions where anisotropy is low because fibers of different tracts merge. The "Lattice" anisotropy index image shows strong contrast between the anisotropic white matter regions and the isotropic gray matter and CSF-filled regions. The Trace image, however, exhibits strong contrast between the CSF-filled regions, where the diffusivity is high, and the gray and white matter regions, where the mean diffusivity is significantly lower.

anisotropy in brain. There, the errors introduced by using rotationally variant diffusion anisotropy measures can be so severe as to preclude their clinical use.

Effect of Noise

Although rotationally invariant diffusion anisotropy measures do not depend on the orientation of the fiber tracts, they are still susceptible to noise contamination. Specifically, noise makes isotropic structures appear anisotropic and makes anisotropic structures appear more anisotropic. In our experiments, the principal diffusivities in all gray matter structures (i.e., putamen, caudate, and parietal cortex) indicate some degree of diffusion anisotropy, since there are statistically significant differences between λ_1 and λ_2, and between λ_2 and λ_3 in all regions (see Table 2). There are also statistically significant differences between λ_2 and λ_3 in all white matter regions. At face value, this result would suggest that water diffusion in the plane perpendicular to fiber-tract axis is not cylindrically symmetric.

Monte Carlo simulations help explain these findings, and more generally how MR image noise affects our measurement of diffusion anisotropy. Sorting the eigenvalues introduces a systematic sampling bias for any non-zero noise level. Figure 4a shows that for all SNR there is a significant difference between the values of λ_1, λ_2, and λ_3 in an isotropic medium, even though their true values (i.e., their asymptotic noise-free values) are all equal. In the presence of background noise, λ_1 is consistently larger than its true value, and λ_3 is consistently smaller than its true value; λ_2 (owing to its symmetric position between the largest and smallest eigenvalues) exhibits the smallest bias.

In Fig. 4b, we see that the systematic sampling bias caused by sorting the eigenvalues has a different effect in anisotropic media. For any non-zero noise level, there is still a significant difference between λ_2 and λ_3, but in white matter, because λ_1 is usually much larger than the other two eigenvalues, the distribution of λ_1 is unlikely to overlap those of λ_2 and λ_3. Therefore, the likelihood of misclassifying λ_1 (even at small SNRs) is much lower in anisotropic media than in isotropic media.

This sorting bias has a profound effect on the anisotropy ratio, λ_1/λ_3. In Fig. 5a we see that λ_1/λ_3 increases as SNR decreases but by a different amount in isotropic and anisotropic media. The variance of λ_1/λ_3 is significantly

Table 4
Comparison among Different Types of Rotationally Invariant Anisotropy Indices

	Corpus callosum	Optic tract	Posterior internal capsule	Anterior internal capsule	Subcortical white matter	Putamen	Caudate	Parietal cortex
λ1/λ3	36.6 ± 37.5	51.8 ± 49.4	61.0 ± 62.2	31.4 ± 89.3	4.5 ± 3.0	1.7 ± 0.3	1.8 ± 0.4	2.0 ± 0.3
λ1/(λ2+λ3)/2	7.4 ± 1.5	9.2 ± 1.7	5.6 ± 1.0	4.6 ± 0.4	2.1 ± 0.3	1.4 ± 0.1	1.5 ± 0.2	1.6 ± 0.1
Fractional anisotropy	0.81 ± 0.07	0.87 ± 0.07	0.77 ± 0.12	0.72 ± 0.04	0.46 ± 0.04	0.24 ± 0.06	0.26 ± 0.07	0.31 ± 0.05
Lattice index	0.57 ± 0.04	0.70 ± 0.03	0.58 ± 0.08	0.53 ± 0.05	0.28 ± 0.02	0.10 ± 0.04	0.11 ± 0.03	0.16 ± 0.04

λ_1/λ_3 and $\lambda_1/(\lambda_2 + \lambda_3)/2$ are intravoxel indices that require sorting of the eigenvalues based on their magnitude. The Fractional Anisotropy index (FA) as well as the Volume Ratio and Relative Anisotropy indices shown in Table 3 are *intravoxel* indices that do not require sorting of the eigenvalues. The noise-immune "lattice" index is an *intervoxel* measure of anisotropy that does not require sorting of the eigenvalues.

larger in anisotropic media than in isotropic media for all SNRs, but the relative bias (estimated value/true value) is larger in isotropic media. Thus, the variance and the bias of λ_1/λ_3 depend on the diffusion properties of the medium. This is clearly undesirable.

It is interesting that the bias predicted by the Monte Carlo simulations is evident in our monkey brain data. Table 2 shows that in white matter, λ_1/λ_3 is inexplicably high (36.6 in the corpus callosum, 51.8 in the optic tract, and 61.0 in the posterior internal capsule), with a large standard deviation. In gray matter (e.g., the putamen, caudate, and parietal cortex), the standard deviation is much lower than that observed in white matter, but the values of λ_1/λ_3 are still significantly different from 1, the value one expects in an isotropic medium.

While in principle, λ_1/λ_3 is an informative measure of anisotropy, in practice it is highly susceptible to noise contamination. There are two reasons for this. First, λ_1/λ_3 does not exploit all of the information contained in the diffusion tensor about anisotropy, so it measures this quantity inefficiently. Second, the bias introduced by sorting the eigenvalues according to their magnitude systematically overestimates λ_1 and underestimates λ_3, making their ratio significantly larger than their true value *at all noise levels*. Functions of λ_1/λ_3, such as the eccentricity, would also be susceptible to this artifact. In conclusion, λ_1/λ_3 should not be used to assess diffusion anisotropy unless an effective means to eliminate its bias and reduce its variance is found.

These problems are partially mitigated by using $\lambda_1/(\lambda_2 + \lambda_3)/2$ instead of λ_1/λ_3 (Fig. 5b). We see that the bias in $\lambda_1/(\lambda_2 + \lambda_3)/2$ is less pronounced, and that it predicts the degree of anisotropy more reliably over a much larger range of SNRs. For isotropic media, the value of $\lambda_1/(\lambda_2 + \lambda_3)/2$ is still significantly different from the true value of 1, because λ_1 and λ_2 are still occasionally misclassified. However, as the degree of anisotropy increases (for the same SNR), the likelihood of misclassifying λ_1 and λ_2 decreases; although individual values of λ_2 and λ_3 are biased, their average is not. $\lambda_1/(\lambda_2 + \lambda_3)/2$ is reasonably accurate and precise for SNR levels greater than 20 when diffusion anisotropy is high. Given that the experimental parameters used in the simulation were identical to those used in the acquisition of the monkey brain images, $\lambda_1/(\lambda_2 + \lambda_3)/2$ provides a good estimate of $D_\parallel/D_\perp$ in highly anisotropic white matter structures at SNR levels typical of our *in vivo* data. However, in our Monte Carlo simulation, we have assumed $\lambda_3 = \lambda_2$. When using $\lambda_1/(\lambda_2 + \lambda_3)/2$ for analysis of the *in vivo* data, one tacitly *assumes* cylindrical symmetry of diffusion in the tissue. This is troubling because there is no evidence to support this assumption in white matter.

The bias introduced by sorting the principal diffusivities is relevant to a number of recent studies. In some studies, it was assumed *a priori* that diffusion in white matter (29), and in skeletal muscle (30, 31) is cylindrically symmetric. Hsu *et al.* (32) recently reported statistically significant differences between the two smallest sorted eigenvalues in skeletal muscle, but still asserted that diffusion in this tissue was cylindrically symmetric. In another interesting study (2), statistically significant differences were observed among the estimated principal diffusivities in cardiac tissue. These were used to support the conclusion that this tissue is not cylindrically symmetric (2). Our analysis suggests that such conflicting claims about the structural and anatomical significance of the sorted eigenvalues can be resolved by accounting for the sorting bias. In general, deciding whether water diffusion in tissue is spherically symmetric (i.e., isotropic), cylindrically symmetric, or asymmetric is a complex statistical problem that cannot be resolved by applying standard statistical tests to the distribution of the *sorted* principal diffusivities in an ROI.

One approach to removing the systematic bias introduced by sorting the eigenvalues is to use a rotationally invariant anisotropy index that is insensitive to their order. This is the case with the Volume Ratio and the Fractional Anisotropy index. Nevertheless, as seen in Fig. 5, at all SNRs, both indices are still slightly biased, making all media appear more anisotropic than they are (although this artifact is no longer caused by sorting). The utility of these anisotropy measures lies in the fact that over the range of SNRs encountered in clinical diffusion imaging studies, their variances are still acceptably small, and relatively insensitive to the degree of anisotropy. For all values of SNR, both of these anisotropy indices are superior to λ_1/λ_3.

Lattice Index

With noisy diffusion-weighted images, the computation of diffusion coefficients is often performed by averaging the diffusion-weighted signals within an anatomical ROI. If our goal is to measure diffusion anisotropy, we generally cannot use this approach, which is only appropriate when the anisotropic structures have the same orientation in all voxels within the anatomical ROI, (i.e., the anisotropy is homogeneous). This requirement may perhaps be satisfied in some skeletal muscles, but it is not satisfied in brain white matter, cardiac muscle (2, 33), intervertebral disk, kidney (4), or other anisotropic tissues in which the fiber orientation of otherwise histologically homogeneous structures can vary dramatically within the anatomical region of interest. Therefore, when imaging these structures, both the diffusion tensor and the anisotropy indices derived from it must be calculated on a voxel-by-voxel basis.

Nonetheless, it is possible to mitigate the effect of noise by using the "lattice" index, without introducing the artifacts caused by averaging the signal intensity over the entire ROI. First, the lattice index is a *local* average, so the likelihood of averaging diffusion tensors whose principal axes of diffusion are oriented in many different directions is reduced. Second, it uses all the information contained in the diffusion tensor to reduce noise (in particular, the eigenvectors of **D**, which are not used explicitly in an intravoxel anisotropy index). Third, it is more immune to bias than an intravoxel index, because the effect of noise, which makes the medium appear more anisotropic, is partially compensated for by the loss in coherence between eigenvectors as the noise level increases. In the simulation results shown in Fig. 5, we see that the lattice anisotropy index significantly reduces

bias, particularly when the degree of anisotropy is low. This is also evident in the images of the monkey brain. By comparing the intravoxel (Fig. 3) and the lattice (Fig. 6) anisotropy measures, we see a dramatic reduction of apparent anisotropy, especially in regions where the signal is low, such as in the muscles surrounding the skull.

One potential disadvantage of using the "lattice" index is that it is not scale invariant, i.e., its value depends on the relative sizes of the voxel and the anatomical structures we want to investigate. If image resolution is low, then the assumption of local homogeneity of the fiber direction field may not be satisfied, and the loss of coherence in the distribution of the eigenvectors will not only be a consequence of the noise, but of anatomical variations as well. It is also important to note that while the lattice index reduces the effect of "random" noise, it will not suppress systematic errors, such as motion artifacts, ghosting, misregistration, distortion of DWIs by eddy currents, miscalibration of the gradients, or errors in the computation of the b-matrix.

In principle, the local averaging process can be further improved by adapting the local averaging window so that it excludes voxels with very different histological characteristics from those of the reference voxel (e.g., at a boundary of CSF and white matter). This local segmentation procedure could employ additional MRI parameters, such as T_1, T_2, Trace(**D**), etc.

Biological Implications

A significant new biological finding reported in this paper is that the anisotropy of white matter in regions where fibers have a regular and parallel arrangement is much higher than was previously reported (34–38). In the most anisotropic structure we investigated, the optic tract, water diffusivity in the direction parallel to fibers is only about a factor of two less than the self-diffusivity of water at body temperature, and almost 10 times larger than the diffusivity in the direction perpendicular to the fibers. This finding is not particular to the monkey brain, since we obtained similar results in cats (39) and in humans (28). We attribute the differences between our findings and those previously reported to differences in methodology. Two factors are primarily responsible: 1) in all previous studies, ADCs were measured rather than the eigenvalues of the diffusion tensor; and 2) the reported spatial resolution in other studies was lower than that used in this study. As discussed above, the degree of anisotropy one measures depends on voxel dimensions, because the larger the voxel, the greater the likelihood of including different tissues (i.e., gray matter or CSF), and the greater the likelihood of including fibers with different orientations.

Another important finding is that diffusion anisotropy is highly variable in different white matter regions; it is much lower in the subcortical white matter than in the optic tract or in the corpus callosum. These differences are not caused by partial volume contamination by gray matter, because at the level of our subcortical ROI, the white matter encompasses a very large region (40). Rather, this disparity arises because the pattern of the fibers in the subcortical regions is less coherent than in the optic tract or in the corpus callosum, where the fibers are parallel. The white matter regions with the lowest diffusion anisotropy are those where different white matter tracts merge. One such area, shown in Fig. 6, lies at the junction of the corpus callosum and the subcortical white matter (arrows); another lies at the junction of the internal capsule and the subcortical white matter (arrows).

While on one hand, these regional differences in white matter anisotropy underscore the utility of this parameter to discriminate between different structural characteristics of tissues, on the other hand, they complicate the interpretation of diffusion anisotropy when used diagnostically. Whereas the values of T_1, T_2, and Trace(**D**) are relatively uniform in normal white matter, the same value of diffusion anisotropy in one anatomical region of white matter could indicate healthy tissue, while in another white matter region it could indicate pathology. Therefore, normal values of the degree of anisotropy must be known in each region. To aid us in this task, a database of normal values of anisotropy should be compiled in different white matter structures for a population of normal subjects.

SUMMARY AND CONCLUSIONS

Measuring the degree of diffusion anisotropy in heterogeneously oriented tissues like brain white matter is more challenging than measuring their average diffusivity or Trace(**D**). We show that rotationally variant measures of diffusion anisotropy, which are calculated directly from apparent diffusion coefficients (ADCs) in two or three perpendicular directions, generally underestimate the degree of diffusion anisotropy in the brain. This orientational artifact can be so severe as to make some highly anisotropic white matter structures appear completely isotropic, indistinguishable from gray matter. Theoretically, we can eliminate this orientational artifact by using rotationally invariant anisotropy indices that are functions of the eigenvalues of the diffusion tensor. Anisotropy measures that require the eigenvalues to be sorted by their magnitude (such as the ratio of the largest and smallest eigenvalues, λ_1/λ_3) are susceptible to a sorting bias that systematically overestimates the degree of diffusion anisotropy. Moreover, once the eigenvalues (and/or eigenvectors) are sorted, the assumptions of random sampling are violated so that standard statistical tests used to analyze their distributions no longer apply.

Other rotationally invariant anisotropy indices can be constructed that are independent of the way we order the eigenvalues. Unfortunately, these anisotropy measures also overestimate the degree of diffusion anisotropy at moderate SNRs, and increasingly so as SNR decreases. However, they are still less susceptible to noise contamination than λ_1/λ_3.

Attempts to increase SNR, either by increasing voxel size or by averaging the signal intensity of DWIs (or diffusion tensors) over a region of interest, introduce a partial volume artifact that causes one to underestimate diffusion anisotropy (by averaging a non-uniform distribution of fiber-tract directions). The lattice index that we propose here is relatively insensitive to this averaging

artifact and significantly decreases both the bias and the variance of the estimated diffusion anisotropy.

The degree of diffusion anisotropy in white matter measured from the diffusion tensor and its variability among different anatomical regions, are significantly higher than was previously reported when ADCs in two or three perpendicular directions were used. In certain structures such as the optic tract, the corpus callosum, and the internal capsule, water diffusivity in the direction parallel to fibers is 7 to 10 times larger than the diffusivity in the direction perpendicular to them, and about a factor of two less than the self-diffusivity of water at body temperature. In other structures, where the pattern of fiber directions is less coherent, anisotropy is much lower and, in some cases, is virtually absent (e.g. in regions where fibers of different bundles merge).

Finally, we want to emphasize that both careful experimental design and the acquisition of high-quality diffusion-weighted images are extremely important to assess the degree of diffusion anisotropy in highly anisotropic and heterogeneously oriented media, such as white matter. The entire diffusion tensor (both diagonal and off-diagonal elements) should be estimated from a relatively large number of low-noise, high-resolution DWIs acquired with a large range of b-matrix values. This systematic and quantitative examination of diffusion anisotropy measures (and of their sources of errors) should help us evaluate the conclusions about diffusion anisotropy drawn in previous MRI studies.

ACKNOWLEDGMENTS

The authors thank Dr. Alan Barnett for helpful discussions about the computation of MR noise, Dr. Giovanni Di Chiro for his support of this collaborative study, and Barry Bowman for editing this manuscript.

REFERENCES

1. G. G. Cleveland, D. C. Chang, C. F. Hazlewood, H. E. Rorschach, Nuclear magnetic resonance measurement of skeletal muscle: anisotrophy of the diffusion coefficient of the intracellular water. *Biophys. J.* **16,** 1043–1053 (1976).
2. T. G. Reese, R. M. Weisskoff, R. Neil Smith, R. Rosen, R. E. Dinsmore, J. van Wedeen, Imaging myocardial fiber architecture in vivo with magnetic resonance. *Magn. Reson. Med.* **34,** 786–791 (1995).
3. Y. Yang, S. Xu, M. J. Dawson, Measurement of water diffusion in hormone-treated rat uteri by diffusion-weighted magnetic resonance imaging. *Magn. Reson. Med.* **33,** 732–735 (1995).
4. M. F. Muller, P. V. Prasad, D. Bimmler, A. Kaiser, R. R. Edelman, Functional imaging of the kidney by means of measurement of the apparent diffusion coefficient. *Radiology* **193,** 711–715 (1994).
5. J. C. Wu, E. C. Wong, E. L. Arrindell, K. B. Simons, A. Jesmanowicz, J. S. Hyde, In vivo determination of the anisotropic diffusion of water and the T1 and T2 times in the rabbit lens by high-resolution magnetic resonance imaging. *Invest. Ophthalmol. Vis. Sci.* **34,** 2151–2158 (1993).
6. M. Doran, J. V. Hajnal, N. Van Bruggen, M. D. King, I. R. Young, G. M. Bydder, Normal and abnormal white matter tracts shown by MR imaging using directional diffusion weighted sequences. *J. Comput. Assist. Tomogr.* **14,** 865–873 (1990).
7. J. V. Hajnal, M. Doran, A. S. Hall, A. G. Collins, A. Oatridge, J. M. Pennock, I. R. Young, G. M. Bydder, MR imaging of anisotropically restricted diffusion of water in the nervous system: technical, anatomic, and pathologic considerations. *J. Comput. Assist. Tomogr.* **15,** 1–18 (1991).
8. M. E. Moseley, Y. Cohen, J. Kucharczyk, J. Mintorovitch, H. S. Asgari, M. F. Wendland, J. Tsuruda, D. Norman, Diffusion-weighted MR imaging of anisotropic water diffusion in cat central nervous system. *Radiology* **176,** 439–445 (1990).
9. P. J. Basser, J. Mattiello, D. LeBihan, MR diffusion tensor spectroscopy and imaging. *Biophys. J.* **66,** 259–267 (1994).
10. B. D. Boss, E. O. Stejskal, Anisotropic diffusion in hydrated vermiculite. *J. Chem. Phys.* **43,** 1068–1069 (1965).
11. P. J. Basser, J. Mattiello, D. LeBihan, Estimation of the effective self-diffusion tensor from the NMR spin echo. *J. Magn. Reson. B* **103,** 247–254 (1994).
12. P. Douek, R. Turner, J. Pekar, N. Patronas, D. Le Bihan, MR color mapping of myelin fiber orientation. *J. Comput. Assist. Tomogr.* **15,** 923–929 (1991).
13. P. van Gelderen, M. H. de Vleeschouwer, D. DesPres, J. Pekar, P. C. van Zijl, C. T. Moonen, Water diffusion and acute stroke. *Magn. Reson. Med.* **31,** 154–163 (1994).
14. C. Pierpaoli, J. Mattiello, D. Le Bihan, G. Di Chiro, P. J. Basser, Diffusion tensor imaging of brain white matter anisotropy, *in* "Proc., SMR, 2nd Meeting, San Francisco, 1994," p. 1038.
15. P. J. Basser, C. Pierpaoli, Microstructural features measured using diffusion tensor imaging. *J. Magn. Reson. B* **111,** 209–219 (1996).
16. E. O. Stejskal, J. E. Tanner, Spin diffusion measurements: spin echoes in the presence of time-dependent field gradient. *J. Chem. Phys.* **42,** 288–292 (1965).
17. D. G. Taylor, M. C. Bushell, The spatial mapping of translational diffusion coefficients by the NMR imaging technique. *Phys. Med. Biol.* **30,** 345–349 (1985).
18. D. Le Bihan, E. Breton, D. Lallemand, P. Grenier, E. Cabanis, M. Laval-Jeantet, MR imaging of intravoxel incoherent motions: application to diffusion and perfusion in neurologic disorders. *Radiology* **161,** 401–407 (1986).
19. J. Mattiello, P. J. Basser, D. LeBihan, Analytical expression for the b matrix in NMR diffusion imaging and spectroscopy. *J. Magn. Reson. A* **108,** 131–141 (1994).
20. P. R. Bevington, "Data Reduction and Error Analysis for the Physical Sciences," New York, McGraw-Hill, 1969.
21. R. M. Henkelman, Measurement of signal intensities in the presence of noise in MR images. *Med. Phys.* **12,** 232–233 (1985).
22. P. J. Basser, Characterizing isotropic and anisotropic diffusion using diffusion tensor MRI. *NMR Biomed.* **8,** 333–344 (1995).
23. T. Nakada, H. Matsuzawa, I. L. Kwee, Magnetic resonance axonography of the rat spinal cord. *Neuroreport* **5,** 2053–2056 (1994).
24. A. J. de Crespigny, M. P. Marks, D. R. Enzmann, M. E. Moseley, Navigated diffusion imaging of normal and ischemic human brain. *Magn. Reson. Med.* **33,** 720–728 (1995).
25. M. Neeman, J. P. Freyer, L. O. Sillerud, Pulsed-gradient spin-echo studies in NMR imaging. Effects of the imaging gradients on the determination of diffusion coefficients. *J. Magn. Reson.* **90,** 303–312 (1990).
26. D. Le Bihan, Molecular diffusion nuclear magnetic resonance imaging. *Magn. Reson. Q.* **7,** 1–30 (1991).
27. P. Jezzard, C. Pierpaoli, Diffusion mapping using interleaved spin echo and STEAM EPI with navigator echo correction, *in* "Proc., SMR, 3rd Annual Meeting, Nice, France, 1995," p. 903.
28. C. Pierpaoli, P. Jezzard, P. J. Basser, High-resolution diffusion tensor imaging of the human brain, *in* "Proc., SMR, 3rd Meeting, Nice, France, 1995," p. 899.
29. J. Coremans, R. Luypaert, F. Verhelle, T. Stadnik, M. Osteaux, A method for myelin fiber orientation mapping using diffusion-weighted MR images. *Magn. Reson. Imaging* **12,** 443–454 (1994).
30. P. van Gelderen, D. DesPres, P. C. van Zijl, C. T. Moonen, Evaluation of restricted diffusion in cylinders. Phosphocreatine in rabbit leg muscle. *J. Magn. Reson. B* **103,** 255–260 (1994).
31. Y. Yang, J. S. Shimony, S. Xu, V. Gulani, M. J. Dawson, P. C. Lauterbur, A sequence for measurement of anisotropic diffusion by projection reconstruction imaging and its application to skeletal and smooth muscle, *in* "Proc., SMR, 2nd Annual Meeting, San Francisco, 1994," p. 1036.
32. E. W. Hsu, S. Mori, Analytical expressions for the NMR apparent diffusion coefficients in an anisotropic system and a simplified method for determining fiber orientation. *Magn. Reson. Med.* **34,** 194–200 (1995).
33. L. Garrido, V. J. Wedeen, K. K. Kwong, U. M. Spencer, H. L. Kantor.

Anisotropy of water diffusion in the myocardium of the rat. *Circ. Res.* **74,** 789–793 (1994).
34. J. A. Brunberg, T. L. Chenevert, P. E. McKeever, D. A. Ross, L. R. Junck, K. M. Muraszko, R. Dauser, J. G. Pipe, A. T. Betley, In vivo MR determination of water diffusion coefficients and diffusion anisotropy: correlation with structural alteration in gliomas of the cerebral hemispheres. *AJNR* **16,** 361–371 (1995).
35. Y. Nomura, H. Sakuma, K. Takeda, T. Tagami, Y. Okuda, T. Nakagawa, Diffusional anisotropy of the human brain assessed with diffusion-weighted MR: relation with normal brain development and aging. *AJNR* **15,** 231–238 (1994).
36. T. L. Chenevert, J. A. Brunberg, J. G. Pipe, Anisotropic diffusion in human white matter: demonstration with MR techniques in vivo. *Radiology* **177,** 401–405 (1990).
37. T. Kajima, K. Azuma, K. Itoh, R. Kagawa, K. Yamane, Y. Okada, T. Shima, Diffusion anisotropy of cerebral ischaemia. *Acta Neurochir. Suppl. (Wien)* **60,** 216–219 (1994).
38. D. Le Bihan, R. Turner, P. Douek, Is water diffusion restricted in human brain white matter? An echo-planar NMR imaging study. *Neuroreport* **4,** 887–890 (1993).
39. C. Pierpaoli, B. Choi, P. Jezzard, P. J. Basser, G. Di Chiro, Significant changes in brain water diffusivity observed under hyperosmolar conditions, *in* "Proc., SMR, 3rd Meeting, Nice, France, 1995," p. 31.
40. J. Szabo, W. M. Cowan, A stereotaxic atlas of the brain of the cynomolgus monkey (Macaca fascicularis). *J. Comp. Neurol.* **222,** 265–300 (1984).